

both for phases associated to nodes and for phases associated to links. Constant phase lags have been traditionally studied in the framework of the Sakaguchi and Kuramoto model [51, 52] which only in the presence of a careful fine tuning of the internal frequencies can lead to non-trivial phase transitions [53, 54]. More recently, space-dependent phase lags have been considered as pivotal elements to describe cortical oscillations [55]. Here we show that time-dependent phase-lags are a natural way to couple dynamical topological signals of nodes and links leading to a very non-trivial phase diagram also for a Gaussian distribution of the internal frequencies.

We investigate the phase diagram of the topological synchronization analytically by extending the Ott-Antonsen approach [56] to treat a dynamics with two order parameters, and by investigating the stability of the steady state solutions of the dynamics. The theoretical results are in perfect agreement with extensive numerical simulations.

The critical properties of topological synchronization are very rich and they include a thermodynamically stable hysteresis loop with a discontinuous forward transition and a continuous downward transition, and a rhythmic phase where the non-zero order parameters are non-stationary. Interestingly, we can predict analytically the critical coupling constant for the discontinuous forward transition and the onset of the instability leading to the rhythmic phase.

Large attention has been recently devoted to investigate which mechanisms are able to induce discontinuous, explosive synchronization transitions [57, 58] in simple networks [59–62], multiplex networks [61, 63–65] and simplicial complexes [24, 66–68].

Interestingly, the discontinuous transition of topological synchronization is driven by the onset of instability of the incoherent phase and leverages on the presence of two order parameters. It results that topological synchronization obeys a topological induced mechanism obtaining an abrupt, discontinuous synchronization transition that cannot be reduced to the recently proposed framework [69] intended to unify the different approaches to explosive synchronization.

The present rhythmic phase is characterized by non-stationary order parameters which emerge at a critical coupling constant whose numerical value we can predict theoretically. The emergent rhythmic phase of topological synchronization extends to a wide range of values of the coupling constant in which very slow oscillations of the order parameters are observed. This phenomenon might shed light over the mechanisms involved in the appearance of brain rhythms and cortical oscillations [10, 55, 70] since Kuramoto like dynamics has been reported to be a very suitable theoretical framework to investigate such brain oscillatory behaviour [55].

Oscillations of the order parameters have been observed in presence of stochastic noise and time delays in Ref [71], in networks with neighbor frequency correlations [72], and in the context of the D -dimensional Ku-

ramoto model [73] in Ref. [74]. However, while in Ref. [74] the magnitude of the order parameter displays large fluctuations, in topological synchronization we have a wide region of the phase diagram in which one of the two complex order parameters (the complex order parameter X_α) oscillates at a low frequency without having large fluctuations of its absolute value, while the other (the complex order parameter X_β) has non-trivial phase and amplitude dynamics. In addition to the explosive forward synchronization transition and the complex rhythmic phase described above the bifurcation diagram of the system features a continuous backward transition, resulting in a very rich phenomenology that could potentially give insight into new mechanisms for the generation of brain rhythms [55].

The paper is organized as follows: in Sec. II we introduce the model of topological synchronization of locally coupled topological signals; in Sec. III we derive the dynamical equations determining the explosive topological synchronization on a fully connected network; in Sec. IV we provide a theoretical treatment of the explosive topological synchronization based on a generalization of the Ott-Antonsen approach; in Sec. V we discuss the phase diagram of the model which displays the explosive discontinuous forward transition and the rhythmic phase; additionally we provide the theoretical predictions obtained by investigating the stability of the steady state solutions and we compare the predictions with extensive numerical simulations; in Sec. VI we discuss the phenomenology characterizing the rhythmic phase of the explosive topological synchronization. Finally, in Sec. VII we provide the concluding remarks.

The paper is enriched by Appendices that give details regarding the correlated internal frequencies of the dynamics of the links projected on the nodes, and provide the theoretical derivations characterizing the stability of the steady state solutions of the model.

II. TOPOLOGICAL SYNCHRONIZATION WITH LOCAL COUPLING

A. Uncoupled synchronization of topological signals

We consider a network $G = (V, E)$ formed by a set of N nodes V and a set of L links E . The topology of the network is captured by the incidence matrix \mathbf{B} mapping any link ℓ of the network to its two endnodes. Specifically, the incidence matrix \mathbf{B} is a rectangular matrix of size $N \times L$ having elements

$$\mathbf{B}_{i\ell} = \begin{cases} 1 & \text{if } \ell = [j, i], \\ -1 & \text{if } \ell = [i, j], \\ 0 & \text{otherwise.} \end{cases} \quad (1)$$

The standard Kuramoto dynamics [1] describes the synchronization of the phases $\boldsymbol{\theta} = (\theta_1, \theta_2, \dots, \theta_N)^\top$ associated to the nodes of the network. In absence of in-

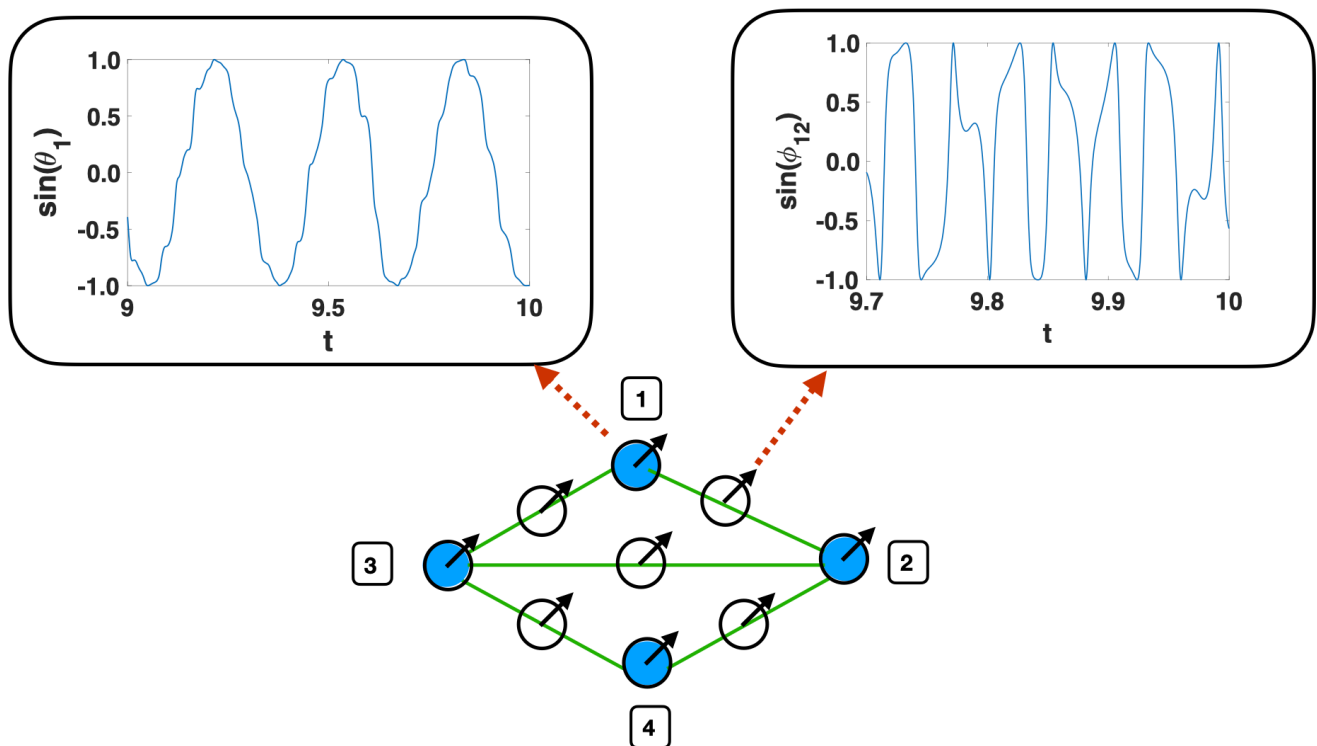


FIG. 1. Schematic representation of topological signals defined on the nodes and the links of a network. Explosive topological synchronization describes the locally coupled dynamics of topological signals defined on nodes and links leading to a discontinuous forward transition and to a coherent rhythmic phase with a non-stationary order parameter.

interactions each phase θ_i oscillates at some intrinsic frequency ω_i drawn typically from a unimodal random distribution. Here we consider the normal distribution $\omega_i \sim \mathcal{N}(\Omega_0, 1/\tau_0)$. However, the phases of next nearest neighbours are coupled to each other by an interaction term that tends to align phases. This term is modulated by a coupling constant $\hat{\sigma}$ that is the control parameter of the dynamics. In terms of the incidence matrix \mathbf{B} the standard Kuramoto model can be expressed as

$$\dot{\boldsymbol{\theta}} = \boldsymbol{\omega} - \hat{\sigma} \mathbf{B} \sin(\mathbf{B}^\top \boldsymbol{\theta}), \quad (2)$$

where $\boldsymbol{\omega} = (\omega_1, \omega_2, \dots, \omega_N)^\top$ indicates the vector of intrinsic frequencies and where with $\sin(\mathbf{x})$ we indicate the vector where the sine function is taken element wise. As a function of the coupling constant the Kuramoto model is known to display a synchronization transition with order parameter

$$R_\theta = \left| \frac{1}{N} \sum_{i=1}^N e^{i\theta_i} \right|. \quad (3)$$

The higher-order Kuramoto model [24] captures synchronization of topological signals (phases) defined on the n -dimensional faces of a simplicial complex, with $n > 0$. On a network, let us consider the topological signals defined on the links determined by the vector phases $\boldsymbol{\phi} = (\phi_{\ell_1}, \phi_{\ell_2}, \dots, \phi_{\ell_L})^\top$. The higher-order Kuramoto dynamics for these phases can be written as

$$\dot{\boldsymbol{\phi}} = \tilde{\boldsymbol{\omega}} - \hat{\sigma} \mathbf{B}^\top \sin(\mathbf{B}\boldsymbol{\phi}), \quad (4)$$

where $\tilde{\boldsymbol{\omega}}$ indicates the vector of internal frequencies of the links, $\tilde{\boldsymbol{\omega}} = (\tilde{\omega}_{\ell_1}, \tilde{\omega}_{\ell_2}, \dots, \tilde{\omega}_{\ell_L})^\top$, with $\tilde{\omega}_\ell \sim \mathcal{N}(\Omega_1, 1/\tau_1)$. The phases associated to the links can be projected to the nodes by applying the incidence matrix that acts like a discrete divergence of the signal defined on the links. The projection of the phases of the links on the nodes is here indicated by $\boldsymbol{\psi}$, and given by

$$\boldsymbol{\psi} = \mathbf{B}\boldsymbol{\phi}. \quad (5)$$

As a function of the coupling constant the higher-order Kuramoto model has been recently shown in Ref. [24] to display a synchronization transition with order parameter

$$R_\psi = \left| \frac{1}{N} \sum_{i=1}^N e^{i\psi_i} \right|. \quad (6)$$

Let us define the Dirac operator [43] of the network as the $(N + L) \times (N + L)$ matrix of block structure

$$\mathcal{D} = \begin{pmatrix} \mathbf{0} & \mathbf{B} \\ \mathbf{B}^\top & \mathbf{0} \end{pmatrix}, \quad (7)$$

whose square is given by the Laplacian operator

$$\mathcal{L} = \mathcal{D}^2 = \begin{pmatrix} \mathbf{L}_{[0]} & \mathbf{0} \\ \mathbf{0} & \mathbf{L}_{[1]} \end{pmatrix}. \quad (8)$$

Here $\mathbf{L}_{[0]} = \mathbf{B}\mathbf{B}^\top$ is the graph Laplacian describing diffusion occurring from node to node through links and

$\mathbf{L}_{[1]} = \mathbf{B}^\top \mathbf{B}$ is the 1-(down)-Laplacian describing the diffusion from link to link through nodes [37, 38].

Using the Dirac operator, the uncoupled dynamics of nodes and links of a network can be written simply as

$$\dot{\Phi} = \Omega - \hat{\sigma} \mathcal{D} \sin(\mathcal{D}\Phi), \quad (9)$$

where Φ and Ω are $N + L$ dimensional column vectors given by

$$\Phi = \begin{pmatrix} \theta \\ \phi \end{pmatrix}, \quad \Omega = \begin{pmatrix} \omega \\ \tilde{\omega} \end{pmatrix}. \quad (10)$$

While the dynamics for the phases associated to the nodes is the standard Kuramoto dynamics that, for the vast majority of network topologies, displays a continuous phase transition at a non-zero value of the coupling constant [4], the dynamics of the higher-order Kuramoto model for the phases associated to the links displays a continuous phase transition for a zero coupling constant [24].

B. Topological synchronization

Having defined the uncoupled dynamics of topological signals defined on nodes and links, given by Eqs. (9), an important question that arises is how these equations can be modified to couple these dynamical equations in non-trivial ways. In Ref. [25] a global adaptive coupling modulating the coupling constant with the order parameters R_θ and R_ψ has been shown to lead to a discontinuous explosive transition of the coupled topological signals. However, it might be argued that physical systems are typically driven by local dynamics. For instance, if the dynamics of nodes and links is assumed to treat brain dynamics it would be easier to justify a local coupling mechanisms rather than a global adaptive dynamics. Here we formulate the equations for topological synchronization of *locally* coupled topological signals defined on nodes and links. We start from the uncoupled Eqs. (9) and we introduce a local adaptive term in the form of a phase lag. We are therefore introducing a phase lag for the node dynamics that depends on the topological signal associated to the nearby links, and vice versa we introduce a phase lag for the links dynamics that depends on the signal on the nodes at its two endpoints. The natural way to introduce these phase lags is by using the Laplacian matrix \mathcal{L} and introduce an appropriate normalization to take into consideration the fact that nodes might have very heterogeneous degree while links are connected always only to the two nodes at their endpoints. Therefore we propose the topological synchronization model driven by the dynamical equations

$$\dot{\Phi} = \Omega - \hat{\sigma} \mathcal{D} \sin(\mathcal{D}\Phi + \gamma \mathcal{K}^{-1} \mathcal{L}\Phi) \quad (11)$$

where the matrix \mathcal{K} is given by

$$\mathcal{K} = \begin{pmatrix} \mathbf{K}_{[0]} & \mathbf{0} \\ \mathbf{0} & \mathbf{K}_{[1]} \end{pmatrix}, \quad (12)$$

i.e., \mathcal{K} is a block-diagonal matrix whose non-zero blocks are formed by the diagonal matrix of node degrees $\mathbf{K}_{[0]}$ and by the diagonal matrix $\mathbf{K}_{[1]}$ of link generalized degrees, indicating the number of nodes connected to each link. Therefore $\mathbf{K}_{[1]}$ has all diagonal elements given by 2. Moreover, in Eq. (11) and in the following we will make use of the matrices γ and \mathcal{I} given by

$$\gamma = \begin{pmatrix} \mathbf{I}_N & \mathbf{0} \\ \mathbf{0} & -\mathbf{I}_L \end{pmatrix} \quad \mathcal{I} = \begin{pmatrix} \mathbf{I}_N & \mathbf{0} \\ \mathbf{0} & \mathbf{I}_L \end{pmatrix}, \quad (13)$$

where \mathbf{I}_X indicates the identity matrix of dimension $X \times X$. It is instructive to write Eq. (11) separately as a dynamical system of equations for the phases θ associated to the nodes and the phases ϕ associated to the links of the network, getting

$$\begin{aligned} \dot{\theta} &= \omega - \hat{\sigma} \mathbf{B} \sin\left(\mathbf{B}^\top \theta + \mathbf{K}_{[1]}^{-1} \mathbf{L}_{[1]} \phi\right), \\ \dot{\phi} &= \tilde{\omega} - \hat{\sigma} \mathbf{B}^\top \sin\left(\mathbf{B} \phi - \mathbf{K}_{[0]}^{-1} \mathbf{L}_{[0]} \theta\right). \end{aligned} \quad (14)$$

This expression reveals explicitly that the coupling between topological signals defined on nodes and links consists of adaptive phase lags determined by the local diffusion properties of the coupled dynamical signals.

Using Eq. (8) we observe that the linearized version of the proposed Eq. (11) still couples nodes and links according to the dynamics

$$\dot{\Phi} = \Omega - \hat{\sigma} (\mathcal{I} + \gamma \mathcal{D} \mathcal{K}^{-1}) \mathcal{L} \Phi. \quad (15)$$

C. Dynamics projected on the nodes

Let us now investigate the dynamical equations that describe the coupled dynamics of the phases ϕ associated to the nodes and the projection ψ of the phases associated to the links, with ψ given by Eq. (5). In terms of the phases θ and ψ the equations dictating the dynamics of the topological synchronization read

$$\begin{aligned} \dot{\theta} &= \omega - \hat{\sigma} \mathbf{B} \sin\left(\mathbf{B}^\top (\theta + \psi/2)\right), \\ \dot{\psi} &= \mathbf{B} \tilde{\omega} - \hat{\sigma} \mathbf{L}_{[0]} \sin\left(\psi - \mathbf{K}_{[0]}^{-1} \mathbf{L}_{[0]} \theta\right), \end{aligned} \quad (16)$$

where we have used the definition of $\mathbf{L}_{[1]} = \mathbf{B}^\top \mathbf{B}$. These equations can be written element wise as

$$\begin{aligned} \dot{\theta}_i &= \omega_i + \hat{\sigma} \sum_{j=1}^N A_{ij} \sin(\alpha_j - \alpha_i), \\ \dot{\psi}_i &= \tilde{\omega}_i - \hat{\sigma} \sum_{j=1}^N A_{ij} [\sin(\beta_j) - \sin(\beta_i)]. \end{aligned} \quad (17)$$

where A_{ij} indicates the generic element of the adjacency matrix \mathbf{A} of the network. Moreover in Eq. (17) we have put

$$\tilde{\omega} = \mathbf{B} \tilde{\omega} \quad (18)$$

and we have defined the variables

$$\begin{aligned}\alpha_i &= \theta_i + \psi_i/2, \\ \beta_i &= \theta_i - \Theta_i - \psi_i,\end{aligned}\quad (19)$$

with

$$\Theta_i = \sum_{j=1}^N \frac{A_{ij}}{k_i} \theta_j. \quad (20)$$

Interestingly, the frequencies $\hat{\omega}$ determined by projecting the internal frequencies of the links $\tilde{\omega}$ on the nodes are correlated even if the frequencies $\tilde{\omega}$ are not (see Appendix A for details).

Although Eqs. (17) can be investigated on an arbitrary (connected) network with adjacency matrix \mathbf{A} , in this paper, however, we will focus on the analytically solvable case in which the network is fully connected.

III. EXPLOSIVE TOPOLOGICAL SYNCHRONIZATION ON A FULLY CONNECTED NETWORK

Here we consider the fully connected network, in which we parametrize the dynamics with the rescaled control parameter $\sigma = \hat{\sigma}/N$ and in which we draw the intrinsic frequencies of the nodes and of the links, respectively, from the distributions $\omega_i \sim \mathcal{N}(\Omega_0, 1)$ and $\tilde{\omega}_\ell \sim \mathcal{N}(0, 1/\sqrt{N-1})$. After considering this rescaling of the parameters, the topological synchronization on a fully connected network admits the projected dynamics given by

$$\begin{aligned}\dot{\theta}_i &= \omega_i + \frac{\sigma}{N} \sum_{j=1}^N \sin(\alpha_j - \alpha_i), \\ \dot{\psi}_i &= \hat{\omega}_i + \sigma \sin(\beta_i) - \frac{\sigma}{N} \sum_{j=1}^N \sin(\beta_j),\end{aligned}\quad (21)$$

where in this case the variables α_i and β_i are defined as

$$\begin{aligned}\alpha_i &= \theta_i + \psi_i/2, \\ \beta_i &= \bar{c}(\theta_i - \hat{\Theta}) - \psi_i,\end{aligned}\quad (22)$$

with $\hat{\Theta}$ given by

$$\hat{\Theta} = \frac{1}{N} \sum_{i=1}^N \theta_i \quad (23)$$

and $\bar{c} = N/(N-1)$. We observe that $\hat{\Theta}$ is the average phase of the nodes of the network that evolves in time at a constant frequency $\hat{\Omega}$ determined only by the intrinsic frequencies of the nodes, in fact, using Eq. (21) we can easily show that

$$\frac{d\hat{\Theta}}{dt} = \frac{1}{N} \sum_{i=1}^N \dot{\theta}_i = \frac{1}{N} \sum_{i=1}^N \omega_i = \hat{\Omega}. \quad (24)$$

Here and in the following we indicate with $G_0(\omega)$ the distribution of intrinsic frequency of each node and with $G_1(\hat{\omega})$ the marginal distribution of the frequencies $\hat{\omega}_i$ for any generic node i of the fully connected network [for the explicit expression of $G_1(\hat{\omega})$ see Appendix B].

In order to study the dynamical Eqs. (21), entirely capturing the topological synchronization on a fully connected network, we introduce the complex order parameters X_α and X_β associated to the phases α_i and β_i of the nodes of the network, i.e.

$$X_\alpha = R_\alpha e^{i\Phi_\alpha} = \frac{1}{N} \sum_{j=1}^N e^{i\alpha_j}, \quad (25)$$

$$X_\beta = R_\beta e^{i\Phi_\beta} = \frac{1}{N} \sum_{j=1}^N e^{i\beta_j}, \quad (26)$$

with R_γ and Φ_γ being real for $\gamma \in \{\alpha, \beta\}$. Using this notation Eq. (21) can also be written as

$$\begin{aligned}\dot{\theta}_i &= \omega_i + \sigma \text{Im} [e^{-i\alpha_i} X_\alpha], \\ \dot{\psi}_i &= \hat{\omega}_i - \sigma \text{Im} X_\beta - \sigma \text{Im} e^{-i\beta_i}.\end{aligned}\quad (27)$$

Since equations (27) are invariant under translation of the α_i variables we consider the transformation

$$\alpha_i \rightarrow \alpha_i - \hat{\Omega}t \quad (28)$$

which guarantees that if X_α is stationary then it is also real, i.e., $X_\alpha = R_\alpha$, simplifying equations (27) to

$$\dot{\alpha}_i = \kappa_i + \sigma \text{Im} [\hat{\mathbf{X}} e^{i\alpha_i}], \quad (29)$$

where we indicate with α_i and $e^{i\alpha_i}$ the vectors

$$\alpha_i = \begin{pmatrix} \alpha_i \\ \beta_i \end{pmatrix}, \quad e^{i\alpha_i} = \begin{pmatrix} e^{-i\alpha_i} \\ e^{-i\beta_i} \end{pmatrix}, \quad (30)$$

and where the vector κ_i and the matrix $\hat{\mathbf{X}}$ in Eq. (29) are given by

$$\begin{aligned}\kappa_i &= \begin{pmatrix} \omega_i - \hat{\Omega} + \hat{\omega}_i/2 - \sigma \text{Im} X_\beta/2 \\ \bar{c}\omega_i - \bar{c}\hat{\Omega} - \hat{\omega}_i + \sigma \text{Im} X_\beta \end{pmatrix}, \\ \hat{\mathbf{X}} &= \begin{pmatrix} X_\alpha & -1/2 \\ \bar{c}X_\alpha & 1 \end{pmatrix}.\end{aligned}\quad (31)$$

IV. THE CONTINUITY EQUATION

A. Generalized Ott-Antonsen approach

In order to study analytically the phase diagram of the topological synchronization determined by the Eqs. (29), let us define the density distribution of $\rho^{(i)}(\alpha, \beta | \omega_i, \hat{\omega}_i)$ of the phases α_i and β_i conditioned on the frequencies ω_i and $\hat{\omega}_i$ as first proposed in [75]. This density distribution satisfies the continuity equation

$$\frac{\partial \rho^{(i)}(\alpha, \beta | \omega_i, \hat{\omega}_i)}{\partial t} + \nabla \cdot \mathbf{J}_i = 0, \quad (32)$$

where the current \mathbf{J}_i is defined as

$$\mathbf{J}_i = \rho^{(i)}(\alpha, \beta | \omega_i, \hat{\omega}_i) \mathbf{v}_i \quad (33)$$

and $\nabla = (\partial_\alpha, \partial_\beta)$. Here the velocity vector \mathbf{v}_i is given by

$$\mathbf{v}_i = \boldsymbol{\kappa}_i + \sigma \text{Im} \left[\hat{\mathbf{X}} e^{i\alpha_i} \right]. \quad (34)$$

In order to solve the continuity equation we extend the Ott-Antonsen [56] approach to this two dimensional case making the ansatz that the Fourier expansion of $\rho^{(i)}(\alpha, \beta | \omega_i, \hat{\omega}_i)$ can be expressed as

$$\rho^{(i)}(\alpha, \beta | \omega, \hat{\omega}) = \frac{1}{(2\pi)^2} \left\{ 1 + \sum_{n>0} \left[f_n^{(\alpha,i)}(\omega, \hat{\omega}, t) e^{in\alpha} + c.c. \right] \right\} \left\{ 1 + \sum_{m>0} \left[f_m^{(\beta,i)}(\omega, \hat{\omega}, t) e^{im\beta} + c.c. \right] \right\}, \quad (35)$$

with

$$\begin{aligned} f_n^{(\alpha,i)}(\omega, \hat{\omega}, t) &= [a_i(\omega, \hat{\omega}, t)]^n \\ f_m^{(\beta,i)}(\omega, \hat{\omega}, t) &= [b_i(\omega, \hat{\omega}, t)]^m \end{aligned} \quad (36)$$

for $n > 0, m > 0$.

For $X_\alpha \neq 0$, $a_i \neq 0$ and $b_i \neq 0$ the continuity equation is satisfied if and only if (see Appendix C for details) a_i and b_i satisfy the system of differential equations

$$\begin{aligned} \partial_t a_i + i a_i \kappa_{\alpha,i} + \frac{1}{2} \sigma [X_\alpha a_i^2 - X_\alpha^*] - \sigma \frac{1}{4} a (b_i - b_i^{-1}) &= 0, \\ \partial_t b_i + i b_i \kappa_{\beta,i} + \frac{1}{2} \sigma \bar{c} [X_\alpha a_i - X_\alpha^* a_i^{-1}] b_i + \sigma \frac{1}{2} (b_i^2 - 1) &= 0, \end{aligned} \quad (37)$$

where here and in the following we indicate with X_α^* the complex conjugate of X_α . In the case in which $X_\alpha = 0$, instead, the continuity equation is satisfied if and only if (see Appendix C for details) a_i and b_i follow the system of differential equations

$$\begin{aligned} \partial_t a_i + i a_i \kappa_{\alpha,i} - \sigma \frac{1}{4} a (b_i - b_i^{-1}) &= 0, \\ \partial_t b_i + i b_i \kappa_{\beta,i} + \sigma \frac{1}{2} (b_i^2 - 1) &= 0. \end{aligned} \quad (38)$$

Let us assume that the frequencies ω_i and $\hat{\omega}_i$ associated to each node i are known. With this hypothesis the complex order parameters can be expressed in terms of the density $\rho^{(i)}(\alpha, \beta | \omega_i, \hat{\omega}_i)$ as

$$\begin{aligned} X_\alpha &= \frac{1}{N} \sum_{i=1}^N \int d\alpha \int d\beta \rho^{(i)}(\alpha, \beta | \omega_i, \hat{\omega}_i) e^{i\alpha}, \\ X_\beta &= \frac{1}{N} \sum_{i=1}^N \int d\alpha \int d\beta \rho^{(i)}(\alpha, \beta | \omega_i, \hat{\omega}_i) e^{i\beta}. \end{aligned} \quad (39)$$

When $\rho^{(i)}(\alpha, \beta | \omega, \hat{\omega})$ satisfies the generalized Ott-Antonsen ansatz given by Eq. (35) and Eq. (36) these

complex order parameters can be expressed in terms of the functions $a_i(\omega_i, \hat{\omega}_i)$ and $b_i(\omega_i, \hat{\omega}_i)$ as

$$\begin{aligned} X_\alpha &= \frac{1}{N} \sum_{i=1}^N a_i^*(\omega_i, \hat{\omega}_i), \\ X_\beta &= \frac{1}{N} \sum_{i=1}^N b_i^*(\omega_i, \hat{\omega}_i), \end{aligned} \quad (40)$$

where a_i^* and b_i^* are the complex conjugates of a_i and b_i , respectively.

If the internal frequencies ω_i and $\hat{\omega}_i$ are not known, we can express these complex order parameters in terms of the marginal distributions $G_0(\omega)$ and $G_1(\hat{\omega})$ as

$$\begin{aligned} X_\alpha &= \int d\omega \int d\hat{\omega} G_0(\omega) G_1(\hat{\omega}) a^*(\omega, \hat{\omega}), \\ X_\beta &= \int d\omega \int d\hat{\omega} G_0(\omega) G_1(\hat{\omega}) b^*(\omega, \hat{\omega}). \end{aligned} \quad (41)$$

Solving the differential equation for $a(\omega, \hat{\omega})$ and $b(\omega, \hat{\omega})$ and using this last expression for the complex order parameter therefore provides a general solution to the topological synchronization dynamics. In the next section we investigate the steady state solution of this dynamics.

B. Steady state solution

Topological synchronization admits two types of stationary solutions: the first one (phase I) is associated with a state in which the phases α_i are incoherent and $R_\alpha = 0$ (but $R_\beta > 0$), and the second one (phase II) is associated to a state with positive order parameters $R_\alpha > 0$ and $R_\beta > 0$. Assuming without loss of generality that in the stationary state the complex order parameter X_α is real, i.e. $X_\alpha = R_\alpha$, and noticing that $R_\alpha > 0$ if and only if not all a_i vanish, the general steady state solution of Eqs. (37) and Eqs. (38) reads

$$a_i = \begin{cases} 0 & \text{in phase I} \\ -id_{i,\alpha} \pm \sqrt{1 - d_{i,\alpha}^2} & \text{in phase II} \end{cases}, \quad (42)$$

$$b_i = -id_{i,\beta} \pm \sqrt{1 - d_{i,\beta}^2}, \quad (43)$$

with

$$d_{i,\alpha} = \frac{\omega_i - \hat{\Omega}}{\sigma R_\alpha}, \quad (44)$$

$$d_{i,\beta} = \begin{cases} \kappa_{i,\beta}/\sigma & \text{in phase I,} \\ -\hat{\omega}_i/\sigma + \text{Im}X_\beta & \text{in phase II.} \end{cases} \quad (45)$$

In order to predict the value of the real order parameters in these two stationary phases let us assume that the frequencies ω_i and $\hat{\omega}_i$ associated to each node i are known. By inserting the expression for the stationary solutions for $a_i(\omega_i, \hat{\omega}_i)$ and $b_i(\omega_i, \hat{\omega}_i)$ given by Eqs. (42)-(43) in Eqs. (40) and imposing that X_α is real, i.e., $X_\alpha = R_\alpha$, we get

$$R_\alpha = \begin{cases} 0 & \text{in phase I} \\ \frac{1}{N} \sum_{i=1}^N \sqrt{1 - d_{i,\alpha}^2} \theta(1 - d_{i,\alpha}^2) & \text{in phase II,} \end{cases} \quad (46)$$

where $\theta(x)$ indicates the Heaviside function. Moreover, the order parameter $X_\beta = R_\beta e^{i\Phi_\beta}$ is determined by the equations

$$R_\beta \cos \Phi_\beta = \frac{1}{N} \sum_{i=1}^N \sqrt{1 - d_{i,\beta}^2} \theta(1 - d_{i,\beta}^2),$$

$$R_\beta \sin \Phi_\beta = \frac{1}{N} \sum_{i=1}^N \left[\sqrt{d_{i,\beta}^2 - 1} \chi(d_{i,\beta}) + d_{i,\beta} \right],$$

where $d_{i,\beta}$ is given by Eqs. (45) and where we have defined the function $\chi(x)$ as

$$\chi(d_{i,\gamma}) = [-\theta(d_{i,\gamma} - 1) + \theta(-1 - d_{i,\gamma})]. \quad (47)$$

Finally, if the projected frequencies ω and $\hat{\omega}$ are not known we can average $a_i^*(\omega, \hat{\omega})$ and $b_i^*(\omega, \hat{\omega})$ appearing in Eqs.(40) over the marginal distributions $G_0(\omega)$ and $G_1(\hat{\omega})$. We observe that the steady state Eqs. (47) always has a solution compatible with $\Phi_\beta = 0$, indicating that the contribution from the phases β_i that are drifting is null. Therefore putting $\Phi_\beta = 0$, we can express the order parameters R_α as $R_\alpha = 0$ in phase I and

$$R_\alpha = \frac{1}{N} \sum_{i=1}^N \int_{|d_{i,\alpha}| \leq 1} d\omega G_0(\omega) \sqrt{1 - d_{i,\alpha}^2}, \quad (48)$$

in phase II, while R_β is given by

$$R_\beta = \frac{1}{N} \sum_{i=1}^N \int_{|d_{i,\beta}| \leq 1} d\hat{\omega} G_1(\hat{\omega}) \sqrt{1 - d_{i,\beta}^2}, \quad (49)$$

in both phase I and phase II as long as $d_{i,\beta}$ is defined by Eq. (45).

V. PHASE DIAGRAM OF TOPOLOGICAL SYNCHRONIZATION

In the previous section we have provided the prediction of the order parameter with the hypothesis that the order parameter reaches a stationary state corresponding to a stable fixed point of the Eqs. (37) and (38). Interestingly, the equations that we have derived for the order parameter R_α [Eq. (48)] are exactly the same as the ones valid for the standard Kuramoto model [1, 3, 5]. Therefore we might naïvely be tempted to assume that the topological synchronization leads to a continuous second order transition at a critical coupling σ_c given by

$$\sigma_c = \frac{2}{\pi G_0(\Omega_0)} = 1.59577 \dots \quad (50)$$

exactly as for the standard Kuramoto model. Surpris-

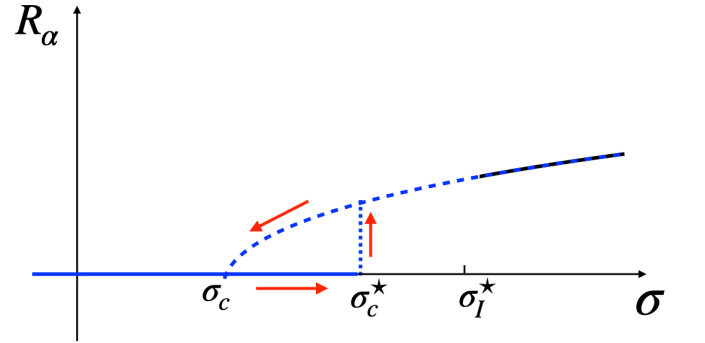


FIG. 2. Schematic representation of the phase diagram indicated by the order parameter R_α versus the coupling constant σ . The steady state solutions are $R_\alpha = 0$ and $R_\alpha > 0$ given by Eq. (48) emerging continuously at σ_c given by Eq. (50). The $R_\alpha = 0$ solution is unstable for $\sigma > \sigma_c^*$ given by Eq. (51). The $R_\alpha > 0$ solution is unstable for $\sigma < \sigma_I^*$ given by Eq. (52). It follows that the topological synchronization displays an hysteresis loop with a discontinuous forward transition and a continuous backward transition, where additionally for $\sigma_c < \sigma < \sigma_I^*$ we observe a rhythmic phase with fluctuations of the order parameter.

ingly, the phase diagram of topological synchronization is much richer and includes a discontinuous forward transition and a rhythmic phase in which the complex order parameters X_α and X_β are not stationary (see schematic representation in Figure 2). In order to capture the real phase diagram of the explosive topological synchronization we need to go beyond the study of the stationary

state solutions of Eqs. (37) and (38) and most notably include the investigations of the stability of these solutions. In the context of the standard Kuramoto model the study of the stability of the incoherent phase puzzled the scientific community for a long time [76, 77] until Strogatz and Mirollo proved in Ref. [75] that σ_c corresponds to the onset of the instability for the incoherent phase, and later Ott and Antonsen [56] revealed the underlying one-dimensional dynamics of the order parameter in the limit $N \rightarrow \infty$.

Here we conduct a stability analysis of the incoherent phase (see Appendix D for the analytical derivations) and we find that surprisingly the incoherent phase becomes unstable only for $\sigma = \sigma_c^* > \sigma_c$ with σ_c^* given by

$$\sigma_c^* = \frac{12}{5} \frac{1}{\pi G_0(\Omega_0)} = 1.91492\dots \quad (51)$$

It follows that topological synchronization displays a discontinuous forward transition at σ_c^* .

The stability analysis around the stationary state of phase II shows an additional notable phenomenon: the onset of a rhythmic phase at σ_I^* where the stationary state of phase II becomes unstable and oscillations of the complex order parameters X_α and X_β emerge. The investigation of the stability of non-trivial solution with R_α given by Eq. (48) can be done by following the same steps used to investigate the stability of the solution $R_\alpha = 0$ (see Appendix E). However, obtaining analytical results is not possible in this case and the investigation needs to be conducted numerically, leading to a numerical value of σ_I^* given by

$$\sigma_I^* = 3.70 \pm 0.05. \quad (52)$$

From this theoretical analysis we expect the phase diagram sketched in Figure 2 displaying a thermodynamically stable hysteresis loop with a discontinuous forward transition at σ_c^* and a continuous backward transition at σ_c , with the onset of the rhythmic phase at σ_I^* .

These theoretical predictions are confirmed by extensive numerical simulations (see Figure 3) of the model defined on a fully connected network of 20,000 nodes (although we can observe some minor instance-to-instance differences). These results are obtained by integrating Eq. (21) with the 4th order Runge-Kutta method with time step $\Delta t = 0.005$ adiabatically increasing and then decreasing the coupling constant σ . From this numerically obtained bifurcation diagram we make the following two observations. First of all, the phase diagram of R_α versus σ does not show large deviations from the predictions obtained by using the stationary solution. As we will see this is due to the fact that in the non-stationary coherent regime X_α changes in time by displaying large oscillations of its global phase while the absolute value of X_α only shows minor fluctuations. Secondly, we notice that the phase diagram of R_β versus σ displays more evident departures from the predictions obtained in the stationary hypothesis in the unstable region. This indicates that in the unstable region X_β has an absolute value

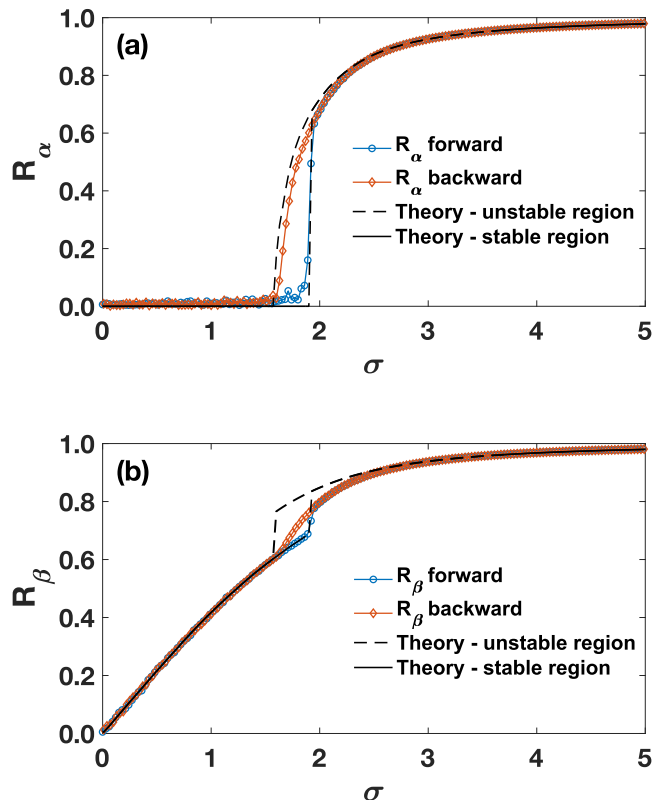


FIG. 3. The forward and backward topological synchronization transitions of the real order parameters R_α (panel (a)) and R_β (panel (b)) are plotted as a function of the coupling constant σ . The numerical results are obtained for a network of $N = 20,000$ nodes, by integrating the dynamical equations with a 4th order Runge-Kutta method with time step $dt = 0.005$ where for each value of σ the dynamics is equilibrated up to time $T_{max} = 10$. The coupling constant σ adiabatically increased and then decreased with steps of size $\Delta\sigma = 0.03$. For each value of σ the plotted values of the real order parameters are averaged over the last fifth of the time series. Black lines indicate the theoretical predictions according to the stationary solutions of the continuity equation. Solid lines indicate stable solutions of the continuity equations and dashed lines indicate unstable solutions of the continuity equation.

that fluctuates and departs from the predictions obtained in the stationary hypothesis. Moreover, we observe that while the predictions obtained under the stationary hypothesis would support also a discontinuous backward transition for R_β , the numerical solutions display a continuous transition. This is in line with the fact that at criticality (i.e., at $\sigma = \sigma_c$) the system is actually in the rhythmic phase, where the hypothesis of stationarity is not valid as predicted in Appendix E.

Finally we observe that this rich phase diagram is only observable by considering the correct order parameters for topological synchronization which are given by R_α and R_β and characterize the synchronization of the coupled topological signals. Indeed, our numerical results

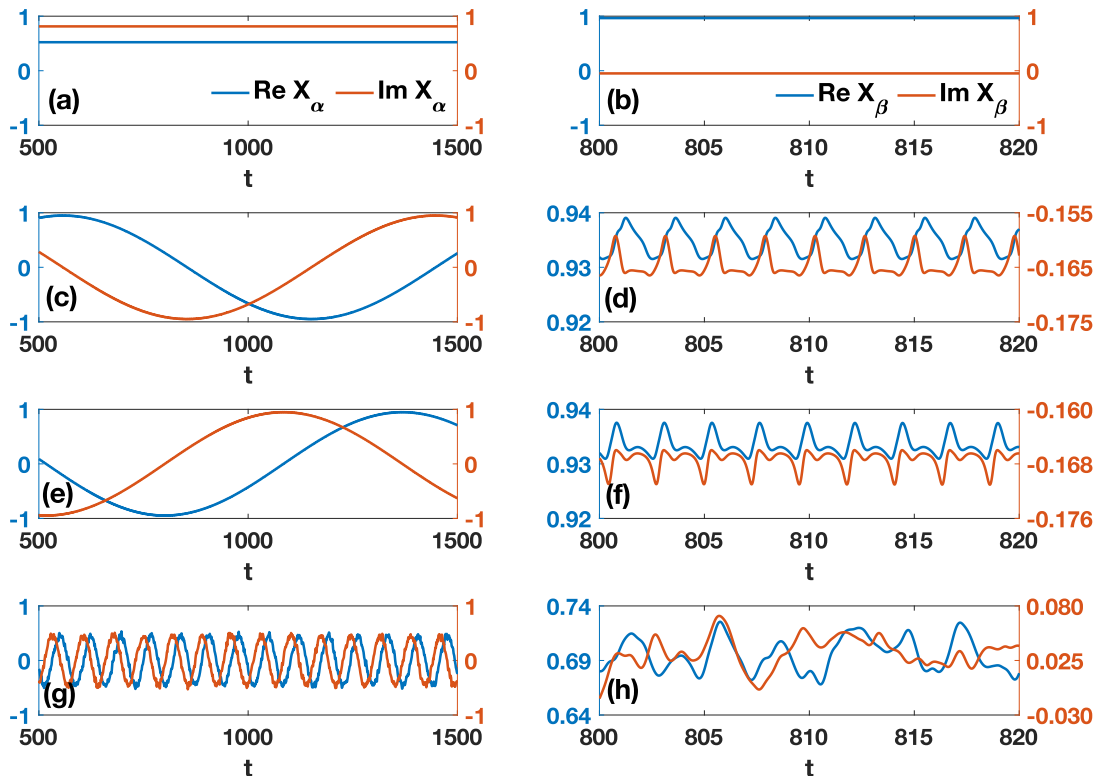


FIG. 4. Post-transient time evolution of the real and imaginary parts of the parameters X_α and X_β . Numerical results are shown for a network of size $N = 500$ during the downward transition. These results are obtained for a network of $N = 500$ nodes with $\sigma = 4$ (panels (a) and (b)), $\sigma = 3.4$ (panels (c) and (d)), for $\sigma = 3.37$ (panels (e) and (f)) and for $\sigma = 1.69$ (panels (g) and (h)).

clearly show that the transition cannot be detected if one considers the naïve uncoupled order parameters R_θ and R_ψ , which remain close to 0 for all values of σ .

VI. NUMERICAL INVESTIGATION OF THE RHYTHMIC PHASE

In this section we investigate numerically the rhythmic phase observed for $\sigma_c < \sigma < \sigma_I^*$ in the backward transition and for $\sigma_c^* < \sigma < \sigma_I^*$ in the forward transition. In this region of the phase space the system is in a non-stationary state where we can no longer assume that X_α and X_β are stationary.

In order to study the dynamical behaviour of the order parameters characterized by a slow fluctuations of the order parameters, we consider a fully connected network of size $N = 500$ where we are able to follow the non-stationary dynamics for very long equilibration time T_{max} .

While for $\sigma > \sigma_I^*$ the order parameters are stationary, in the rhythmic phase the order parameters do not reach a stable fixed point and their real and imaginary parts undergo fluctuations as shown in Figure 4. In particular, we are able to show that close to the onset of the

rhythmic phase σ_I^* the order parameter X_α displays a slow rotation in the complex plane with constant angular frequency and constant absolute value of $|X_\alpha| = R_\alpha$, while X_β performs a periodic motion along a closed limit cycle. If the value of the coupling constant is decreased, first the order parameter X_β displays a more complex dynamics while X_α continues to oscillate at essentially constant absolute value R_α . Then, as σ approaches σ_c higher frequency oscillations of the magnitude of X_α also set in. The phase space portraits corresponding to the dynamics of the complex order parameters presented in Figure 4 are shown in Figure 5, revealing the nature of the fluctuations of the order parameters.

The dynamics of the complex order parameter X_α is particularly interesting in relation to the study of brain rhythms and cortical oscillations which have their origin in the level of synchronization within neuronal populations or cortical areas. In order to describe the non-trivial dynamical behavior of X_α during the backward transition we show in Figure 6 the phase portrait of X_α when the coupling constant σ is decreased in time in a fully connected network of size $N = 500$, where at each value of the coupling constant the dynamics is equilibrated for a time $T_{max} = 10$. From this figure it is apparent that for $\sigma_c < \sigma < \sigma_I^*$ the order parameter X_α displays slow fre-

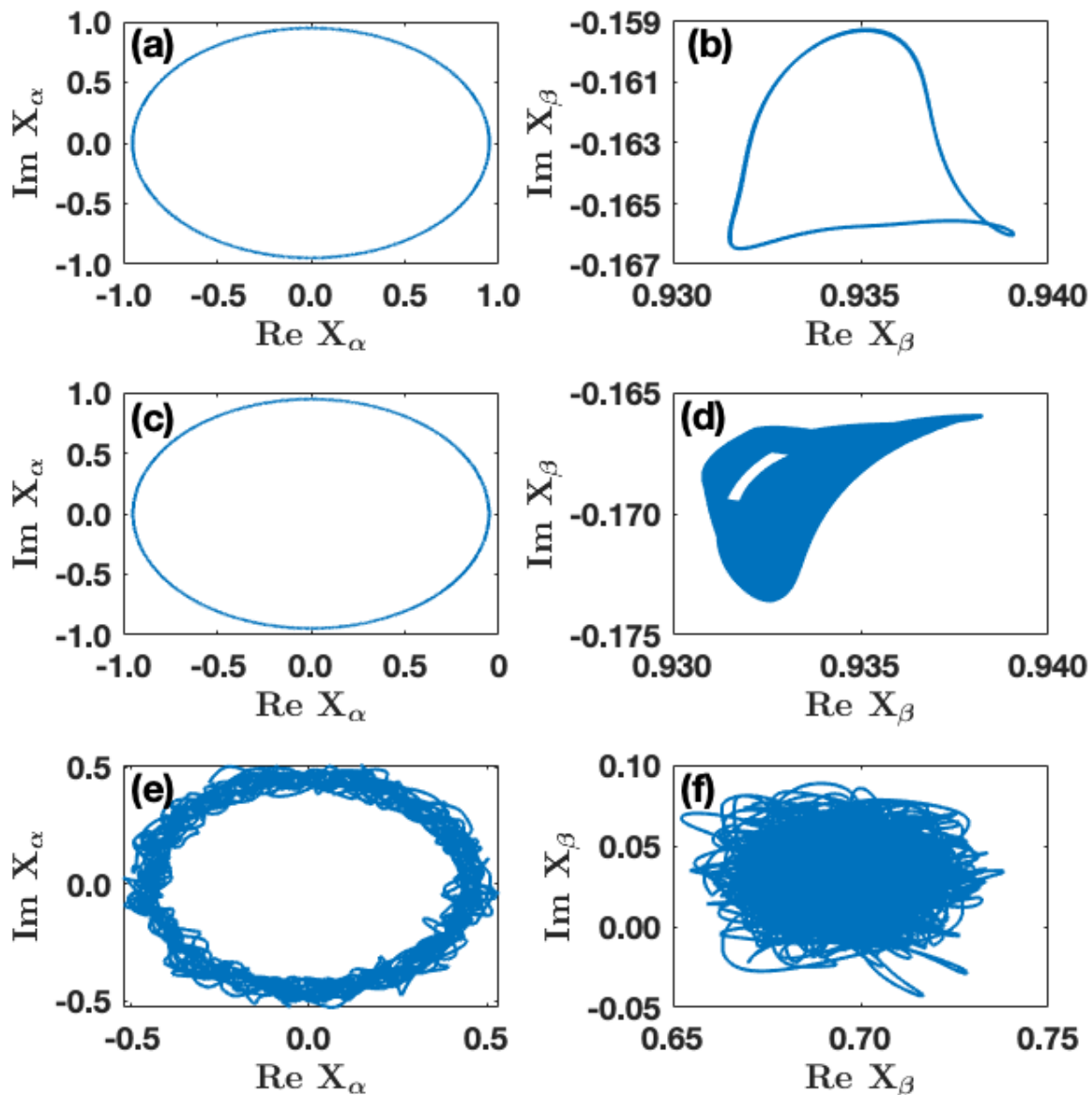


FIG. 5. The trajectories of the real and imaginary parts of the complex order parameters X_α and X_β are displayed for different values of the coupling constant σ in the backward transition. These results are obtained by neglecting the transient, from a network of $N = 500$ nodes with $\sigma = 3.4$ (panel (a) and (b)), with $\sigma = 3.37$ (panel (c) and (d)) and with $\sigma = 1.69$ (panel (e) and (f)).

quency oscillations with an amplitude that decreases as the coupling constant σ is decreased. Moreover, the figure shows that the amplitude displays smaller and faster frequency fluctuations that becomes more significant as the coupling constant approaches σ_c .

VII. CONCLUSIONS

In this work we have formulated and discussed the explosive topological synchronization of locally coupled topological signals associated to the nodes and to the links of a network. Topological signals associated to

nodes are traditionally studied in models of non-linear dynamics of a network, however the dynamics of topological signals associated to the links of the network is so far much less explored.

In brain and neuronal networks, the topological signals of the links can be associated to a dynamical state of synapses (for example oscillatory signals associated to intracellular calcium dynamics involved in synaptic communication among neurons [46]), and more generally they can be associated to dynamical weights or fluxes associated to the links of the considered network. The considered coupling mechanism between topological signals of nodes and links is local, meaning that every node and ev-

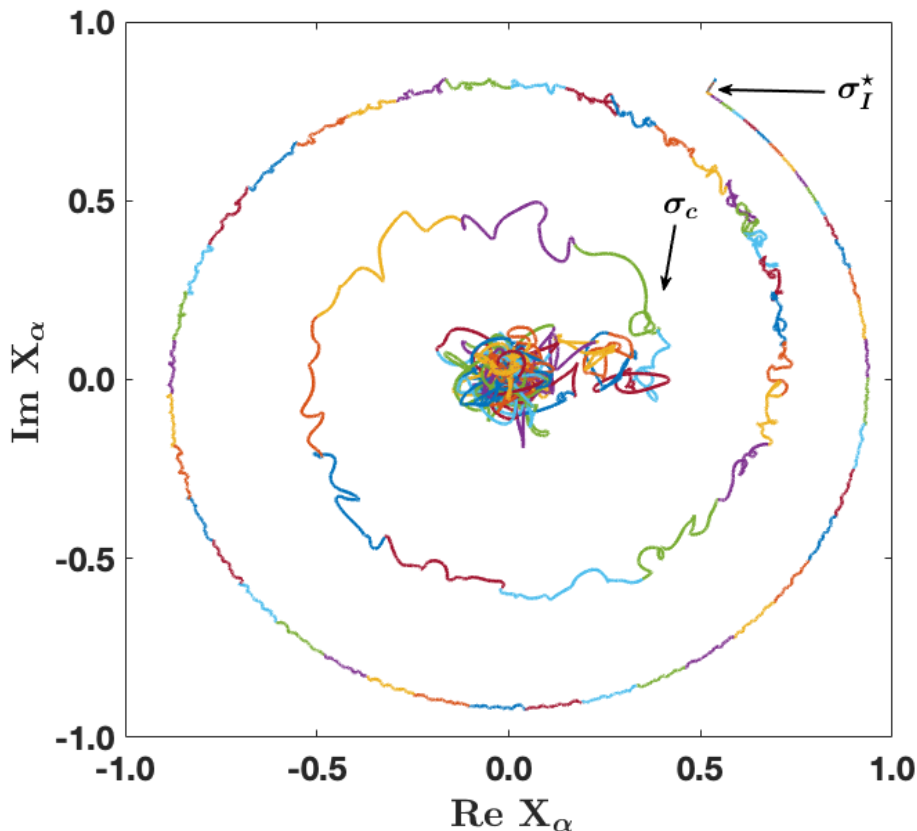


FIG. 6. The evolution of the complex order parameter X_α during the backward synchronization transition is plotted for different values of the coupling constant σ as the coupling constant decreases (indicated by colors of different lines). This simulation results have been obtained for a network of $N = 500$, $T_{max} = 10$, and $\delta\sigma = 0.03$. The onset of the instability of the steady state solution at σ_I^* and the onset on the incoherent phase at σ_c are indicated by the arrows.

ery link is only affected by the dynamics of nearby nodes and links. In particular, the dynamics of the nodes is dictated by a Kuramoto-like system of equations where we introduce a phase lag that depends on the dynamical state of nearby links and, similarly, the dynamics of the links is dictated by a higher-order Kuramoto-like system of equations [24] where we introduce a phase lag dependent on the dynamical state of nearby nodes.

On a fully connected network, topological synchronization is explosive as it leads to a discontinuous forward synchronization transition and a continuous backward synchronization transition. Therefore, topological synchronization determines a topological mechanism to achieve abrupt discontinuous synchronization transitions. The theoretical investigation of the model predicts that the discontinuous transition occurs at a theoretically predicted value of the coupling constant σ_c^* when the incoherent phase loses stability. However, for smaller value of the coupling constant the incoherent phase can coexist with the coherent one.

The coherent phase can be observed for $\sigma > \sigma_c$ where σ_c is the synchronization threshold of the standard Kuramoto model [1, 3], however for $\sigma < \sigma_I^*$ the system is in a rhythmic phase characterized by non-stationary order

parameters. Here we theoretically predict the numerical value of σ_I^* and we investigate numerically the dynamics of the order parameters in the rhythmic phase.

This work shows how topology can be combined with dynamical systems leading to a new framework to capture abrupt synchronization transitions and the emergence of non trivial rhythmic phases.

This work can be extended in different directions. First of all the model can be applied to more complex network topologies including not only random graphs and scale-free networks but also real network topologies such as experimentally obtained brain networks. Secondly, using the higher-order Dirac operator [43] topological synchronization can be extended to simplicial complexes where topological signals can be defined also on higher-order simplices such as triangles, tetrahedra and so on. We hope that this work will stimulate further theoretical and applied research along these lines.

ACKNOWLEDGMENTS

This work is partially supported by SUPERSTRIPES Onlus. This research utilized Queen Mary's Apoc-

rita HPC facility, supported by QMUL Research-IT. <http://doi.org/10.5281/zenodo.438045>. G.B. acknowledges support from Royal Society IEC\NSFC\191147. J.J.T. acknowledges financial support from the Con-

sejería de Transformación Económica, Industria, Conocimiento y Universidades, Junta de Andalucía and European Regional Development Funds, Ref. P20_00173.

-
- [1] Yoshiki Kuramoto, “Self-entrainment of a population of coupled non-linear oscillators,” in *International Symposium on Mathematical Problems in Theoretical Physics*, edited by Huzihiro Araki (Springer Berlin Heidelberg, Berlin, Heidelberg, 1975) pp. 420–422.
- [2] Steven H Strogatz, *Nonlinear dynamics and chaos with student solutions manual: With applications to physics, biology, chemistry, and engineering* (CRC Press, 2018).
- [3] Steven H Strogatz, “From kuramoto to crawford: exploring the onset of synchronization in populations of coupled oscillators,” *Physica D: Nonlinear Phenomena* **143**, 1–20 (2000).
- [4] Alex Arenas, Albert Díaz-Guilera, Jurgen Kurths, Yamir Moreno, and Changsong Zhou, “Synchronization in complex networks,” *Physics Reports* **469**, 93–153 (2008).
- [5] Stefano Boccaletti, Alexander N Pisarchik, Charo I Del Genio, and Andreas Amann, *Synchronization: from coupled systems to complex networks* (Cambridge University Press, 2018).
- [6] Arkady Pikovsky, Jurgen Kurths, Michael Rosenblum, and Jürgen Kurths, *Synchronization: a universal concept in nonlinear sciences*, 12 (Cambridge University Press, 2003).
- [7] Steven H Strogatz, *Sync: How order emerges from chaos in the universe, nature, and daily life* (Hachette UK, 2012).
- [8] Thilo Gross, “Not one, but many critical states: A dynamical systems perspective,” *Frontiers in Neural Circuits* **15**, 7 (2021).
- [9] Leon Glass and Michael C Mackey, *From clocks to chaos* (Princeton University Press, 2020).
- [10] Gyorgy Buzsáki, *Rhythms of the Brain* (Oxford University Press, 2006).
- [11] Iain D Couzin, “Synchronization: the key to effective communication in animal collectives,” *Trends in Cognitive Sciences* **22**, 844–846 (2018).
- [12] Kurt Wiesenfeld, Pere Colet, and Steven H Strogatz, “Frequency locking in josephson arrays: Connection with the kuramoto model,” *Physical Review E* **57**, 1563 (1998).
- [13] Miguel C Soriano, Jordi García-Ojalvo, Claudio R Mirasso, and Ingo Fischer, “Complex photonics: Dynamics and applications of delay-coupled semiconductor lasers,” *Reviews of Modern Physics* **85**, 421 (2013).
- [14] Bihui Zhu, Johannes Schachenmayer, Minghui Xu, F Herrera, Juan G Restrepo, Murray J Holland, and Ana Maria Rey, “Synchronization of interacting quantum dipoles,” *New Journal of Physics* **17**, 083063 (2015).
- [15] Dirk Witthaut, Sandro Wimberger, Raffaella Burioni, and Marc Timme, “Classical synchronization indicates persistent entanglement in isolated quantum systems,” *Nature Communications* **8**, 1–7 (2017).
- [16] Mikio Nakahara, *Geometry, topology and physics* (CRC Press, 2003).
- [17] Chen Ning Yang, Mo-Lin Ge, and Yang-Hui He, *Topology and Physics* (World Scientific, 2019).
- [18] John Michael Kosterlitz and David James Thouless, “Ordering, metastability and phase transitions in two-dimensional systems,” *Journal of Physics C: Solid State Physics* **6**, 1181 (1973).
- [19] Suraj Shankar, Anton Souslov, Mark J Bowick, M Cristina Marchetti, and Vincenzo Vitelli, “Topological active matter,” arXiv preprint arXiv:2010.00364 (2020).
- [20] Shun-Qing Shen, *Topological insulators*, Vol. 174 (Springer, 2012).
- [21] Michel Fruchart and David Carpentier, “An introduction to topological insulators,” *Comptes Rendus Physique* **14**, 779–815 (2013).
- [22] Evelyn Tang, Jaime Agudo-Canalejo, and Ramin Golestanian, “Topology protects chiral edge currents in stochastic systems,” arXiv preprint arXiv:2010.02845 (2020).
- [23] Ana Paula Millán, Juan G Restrepo, Joaquín J Torres, and Ginestra Bianconi, “Geometry, topology and simplicial synchronization,” arXiv preprint arXiv:2105.00943 (2021).
- [24] Ana P Millán, Joaquín J Torres, and Ginestra Bianconi, “Explosive higher-order kuramoto dynamics on simplicial complexes,” *Physical Review Letters* **124**, 218301 (2020).
- [25] Reza Ghorbanchian, Juan G Restrepo, Joaquín J Torres, and Ginestra Bianconi, “Higher-order simplicial synchronization of coupled topological signals,” arXiv preprint arXiv:2011.00897 (2020).
- [26] Joseph D Hart, Yuanzhao Zhang, Rajarshi Roy, and Adilson E Motter, “Topological control of synchronization patterns: Trading symmetry for stability,” *Physical Review Letters* **122**, 058301 (2019).
- [27] Federico Battiston, Giulia Cencetti, Iacopo Iacopini, Vito Latora, Maxime Lucas, Alice Patania, Jean-Gabriel Young, and Giovanni Petri, “Networks beyond pairwise interactions: structure and dynamics,” *Physics Reports* (2020).
- [28] Christian Bick, Elizabeth Gross, Heather A Harrington, and Michael T Schaub, “What are higher-order networks?” arXiv preprint arXiv:2104.11329 (2021).
- [29] Chad Giusti, Robert Christ, and Danielle S Bassett, “Two’s company, three (or more) is a simplex,” *Journal of Computational Neuroscience* **41**, 1–14 (2016).
- [30] Nina Otter, Mason A Porter, Ulrike Tillmann, Peter Grindrod, and Heather A Harrington, “A roadmap for the computation of persistent homology,” *EPJ Data Science* **6**, 1–38 (2017).
- [31] Jürgen Jost, *Mathematical concepts* (Springer, 2015).
- [32] Dane Taylor, Florian Klimm, Heather A Harrington, Miroslav Kramár, Konstantin Mischaikow, Mason A Porter, and Peter J Mucha, “Topological data analysis of contagion maps for examining spreading processes on networks,” *Nature Communications* **6**, 1–11 (2015).

- [33] Raffaella Mulas, Christian Kuehn, and Jürgen Jost, “Coupled dynamics on hypergraphs: master stability of steady states and synchronization,” *Physical Review E* **101**, 062313 (2020).
- [34] Alice Patania, Francesco Vaccarino, and Giovanni Petri, “Topological analysis of data,” *EPJ Data Science* **6**, 1–6 (2017).
- [35] Giovanni Petri, Paul Expert, Federico Turkheimer, Robin Carhart-Harris, David Nutt, Peter J Hellyer, and Francesco Vaccarino, “Homological scaffolds of brain functional networks,” *Journal of The Royal Society Interface* **11**, 20140873 (2014).
- [36] Danijela Horak and Jürgen Jost, “Spectra of combinatorial laplace operators on simplicial complexes,” *Advances in Mathematics* **244**, 303–336 (2013).
- [37] Joaquín J Torres and Ginestra Bianconi, “Simplicial complexes: higher-order spectral dimension and dynamics,” *Journal of Physics: Complexity* **1**, 015002 (2020).
- [38] Sergio Barbarossa and Stefania Sardellitti, “Topological signal processing over simplicial complexes,” *IEEE Transactions on Signal Processing* **68**, 2992–3007 (2020).
- [39] Michael T Schaub, Austin R Benson, Paul Horn, Gabor Lippner, and Ali Jadbabaie, “Random walks on simplicial complexes and the normalized Hodge 1-Laplacian,” *SIAM Review* **62**, 353–391 (2020).
- [40] Michael T Schaub, Yu Zhu, Jean-Baptiste Seby, T Mitchell Roddenberry, and Santiago Segarra, “Signal processing on higher-order networks: Livin’ on the edge... and beyond,” *arXiv preprint arXiv:2101.05510* (2021).
- [41] Stefania Ebli, Michaël Defferrard, and Gard Spreemann, “Simplicial neural networks,” *arXiv preprint arXiv:2010.03633* (2020).
- [42] Cristian Bodnar, Fabrizio Frasca, Yu Guang Wang, Nina Otter, Guido Montúfar, Pietro Lio, and Michael Bronstein, “Weisfeiler and lehman go topological: Message passing simplicial networks,” *arXiv preprint arXiv:2103.03212* (2021).
- [43] Ginestra Bianconi, “The topological dirac equation of networks and simplicial complexes,” *arXiv preprint arXiv:2106.02929* (2021).
- [44] Lee DeVille, “Consensus on simplicial complexes: Results on stability and synchronization,” *Chaos: An Interdisciplinary Journal of Nonlinear Science* **31**, 023137 (2021).
- [45] Geneviève Dupont, Laurent Combettes, Gary S Bird, and James W Putney, “Calcium oscillations,” *Cold Spring Harbor perspectives in biology* **3**, a004226 (2011).
- [46] Lucia Pasti, Andrea Volterra, Tullio Pozzan, and Giorgio Carmignoto, “Intracellular calcium oscillations in astrocytes: A highly plastic, bidirectional form of communication between neurons and astrocytes in situ,” *Journal of Neuroscience* **17**, 7817–7830 (1997).
- [47] Weiyu Huang, Thomas AW Bolton, John D Medaglia, Danielle S Bassett, Alejandro Ribeiro, and Dimitri Van De Ville, “A graph signal processing perspective on functional brain imaging,” *Proceedings of the IEEE* **106**, 868–885 (2018).
- [48] Jason W Rocks, Andrea J Liu, and Eleni Katifori, “Hidden topological structure of flow network functionality,” *Physical Review Letters* **126**, 028102 (2021).
- [49] Eleni Katifori, Gergely J Szöllösi, and Marcelo O Magasco, “Damage and fluctuations induce loops in optimal transport networks,” *Physical Review Letters* **104**, 048704 (2010).
- [50] Franz Kaiser, Henrik Ronellenfitsch, and Dirk Witthaut, “Discontinuous transition to loop formation in optimal supply networks,” *Nature Communications* **11**, 1–11 (2020).
- [51] Hidetsugu Sakaguchi and Yoshiki Kuramoto, “A soluble active rotator model showing phase transitions via mutual entertainment,” *Progress of Theoretical Physics* **76**, 576–581 (1986).
- [52] Lars Q English, Zhuwei Zeng, and David Mertens, “Experimental study of synchronization of coupled electrical self-oscillators and comparison to the sakaguchi-kuramoto model,” *Physical Review E* **92**, 052912 (2015).
- [53] E Omel’chenko and Matthias Wolfrum, “Nonuniversal transitions to synchrony in the sakaguchi-kuramoto model,” *Physical Review Letters* **109**, 164101 (2012).
- [54] E Omel’chenko and Matthias Wolfrum, “Bifurcations in the sakaguchi-kuramoto model,” *Physica D: Nonlinear Phenomena* **263**, 74–85 (2013).
- [55] Michael Breakspear, Stewart Heitmann, and Andreas Daffertshofer, “Generative models of cortical oscillations: neurobiological implications of the kuramoto model,” *Frontiers in human neuroscience* **4**, 190 (2010).
- [56] Edward Ott and Thomas M Antonsen, “Low dimensional behavior of large systems of globally coupled oscillators,” *Chaos: An Interdisciplinary Journal of Nonlinear Science* **18**, 037113 (2008).
- [57] S Boccaletti, JA Almendral, S Guan, I Leyva, Z Liu, I Sendiña-Nadal, Z Wang, and Y Zou, “Explosive transitions in complex networks’ structure and dynamics: Percolation and synchronization,” *Physics Reports* **660**, 1–94 (2016).
- [58] Raissa M D’Souza, Jesus Gómez-Gardeñes, Jan Nagler, and Alex Arenas, “Explosive phenomena in complex networks,” *Advances in Physics* **68**, 123–223 (2019).
- [59] Jesús Gómez-Gardenes, Sergio Gómez, Alex Arenas, and Yamir Moreno, “Explosive synchronization transitions in scale-free networks,” *Physical Review Letters* **106**, 128701 (2011).
- [60] BC Coutinho, AV Goltsev, SN Dorogovtsev, and JFF Mendes, “Kuramoto model with frequency-degree correlations on complex networks,” *Physical Review E* **87**, 032106 (2013).
- [61] Xiyun Zhang, Stefano Boccaletti, Shuguang Guan, and Zonghua Liu, “Explosive synchronization in adaptive and multilayer networks,” *Physical Review Letters* **114**, 038701 (2015).
- [62] Xiyun Zhang, Xin Hu, Jürgen Kurths, and Zonghua Liu, “Explosive synchronization in a general complex network,” *Physical Review E* **88**, 010802 (2013).
- [63] Vincenzo Nicosia, Per Sebastian Skardal, Alex Arenas, and Vito Latora, “Collective phenomena emerging from the interactions between dynamical processes in multiplex networks,” *Physical Review Letters* **118**, 138302 (2017).
- [64] Ajay Deep Kachhvah and Sarika Jalan, “Delay regulated explosive synchronization in multiplex networks,” *New Journal of Physics* **21**, 015006 (2019).
- [65] Sarika Jalan, Vasundhara Rathore, Ajay Deep Kachhvah, and Alok Yadav, “Inhibition-induced explosive synchronization in multiplex networks,” *Physical Review E* **99**, 062305 (2019).
- [66] Per Sebastian Skardal and Alex Arenas, “Abrupt desynchronization and extensive multistability in globally coupled oscillator simplexes,” *Physical Review Letters* **122**,

- 248301 (2019).
- [67] Per Sebastian Skardal and Alex Arenas, “Higher order interactions in complex networks of phase oscillators promote abrupt synchronization switching,” *Communications Physics* **3**, 1–6 (2020).
- [68] Maxime Lucas, Giulia Cencetti, and Federico Battiston, “Multiorder laplacian for synchronization in higher-order networks,” *Physical Review Research* **2**, 033410 (2020).
- [69] Christian Kuehn and Christian Bick, “A universal route to explosive phenomena,” *Science Advances* **7**, eabe3824 (2021).
- [70] Joana Cabral, Etienne Hugues, Olaf Sporns, and Gustavo Deco, “Role of local network oscillations in resting-state functional connectivity,” *Neuroimage* **57**, 130–139 (2011).
- [71] MK Stephen Yeung and Steven H Strogatz, “Time delay in the kuramoto model of coupled oscillators,” *Physical Review Letters* **82**, 648 (1999).
- [72] Juan G Restrepo and Edward Ott, “Mean-field theory of assortative networks of phase oscillators,” *EPL (Europhysics Letters)* **107**, 60006 (2014).
- [73] Sarthak Chandra, Michelle Girvan, and Edward Ott, “Continuous versus discontinuous transitions in the d-dimensional generalized kuramoto model: Odd d is different,” *Physical Review X* **9**, 011002 (2019).
- [74] X Dai, X Li, H Guo, D Jia, M Perc, P Manshour, Z Wang, and S Boccaletti, “Discontinuous transitions and rhythmic states in the d-dimensional kuramoto model induced by a positive feedback with the global order parameter,” *Physical Review Letters* **125**, 194101 (2020).
- [75] Steven H Strogatz and Renato E Mirollo, “Stability of incoherence in a population of coupled oscillators,” *Journal of Statistical Physics* **63**, 613–635 (1991).
- [76] Yoshiki Kuramoto and Ikuko Nishikawa, “Statistical macrodynamics of large dynamical systems. case of a phase transition in oscillator communities,” *Journal of Statistical Physics* **49**, 569–605 (1987).
- [77] F Kuramoto and I Nishikawa, “Onset of collective rhythms in large populations of coupled oscillators,” in *Cooperative Dynamics in Complex Physical Systems* (Springer, 1989) pp. 300–306.

Appendix A: Internal frequencies of the projected dynamics

The frequencies $\hat{\omega}$ determining the uncoupled dynamics of the variables ψ can be determined starting from the internal frequencies of the links $\tilde{\omega}$ according to Eq. (18). In particular, since the frequencies $\tilde{\omega}$ are normally distributed, the frequencies $\hat{\omega}$ will also be normally distributed. However the Eq.(18) implies that the frequencies $\hat{\omega}$ are correlated.

Using the definition of the incidence matrix \mathbf{B} it is easy to show that the expectation of $\hat{\omega}_i$ is given by

$$\langle \hat{\omega}_i \rangle = \left[\sum_{j < i} A_{ij} - \sum_{j > i} A_{ij} \right] \Omega_1. \quad (\text{A1})$$

Given that each node has degree k_i , the covariance matrix \mathbf{C} is given by the graph Laplacian $\mathbf{L}_{[0]}$ of the

network, i.e.

$$\begin{aligned} C_{ij} &= \langle \hat{\omega}_i \hat{\omega}_j \rangle_c = \sum_{\ell, \ell'} \langle [\mathbf{B}\tilde{\omega}]_i [\mathbf{B}\tilde{\omega}]_j \rangle_c \\ &= [L_{[0]}]_{ij} \frac{1}{\tau_1^2} = [k_i \delta_{ij} - A_{ij}] \frac{1}{\tau_1^2}, \end{aligned} \quad (\text{A2})$$

where we have indicated with $\langle \dots \rangle_c$ the connected correlation. Moreover we note that the average of $\hat{\omega}$ over all the nodes of the network is zero. In fact

$$\sum_{i=1}^N \hat{\omega}_i = \mathbf{1}^T \hat{\omega} = \mathbf{1}^T \mathbf{B} \omega = 0, \quad (\text{A3})$$

where here with $\mathbf{1}$ we indicate the N -dimensional column vector of elements $1_i = 1$. Finally by using the symmetry of the adjacency matrix, i.e. the fact that $A_{ij} = A_{ji}$, we can show that Eq. (A3) implies that the sum of ψ_i over all the nodes of the network is zero, i.e.

$$\sum_{i=1}^N \dot{\psi}_i = \sum_{i=1}^N \hat{\omega}_i - \hat{\sigma} \sum_{i,j} A_{ij} [\sin \beta_i - \sin \beta_j] = 0. \quad (\text{A4})$$

Appendix B: Rescaling of the parameters for topological synchronization on a fully connected network

Eq. (11) or equivalently Eq. (17) define topological synchronization in a network with adjacency matrix \mathbf{A} . If we focus on a fully connected network, in order to have well defined phases in the large network limit, we need to consider an opportune rescaling of the coupling constant and we put

$$\hat{\sigma} = \sigma/N. \quad (\text{B1})$$

We also need to adopt suitable rescaling of the parameters determining the distribution of the internal frequencies of the nodes and of the links. The internal frequencies of nodes ω are taken to be independent Gaussian variables

$$\omega_i \sim \mathcal{N}(\Omega_0, 1) \quad (\text{B2})$$

for each node i of the network. For simplicity the internal frequencies of the links $\tilde{\omega}$ are taken to be independent Gaussian variables with zero average, and standard deviation $1/\sqrt{N-1}$, i.e.

$$\tilde{\omega}_\ell \sim \mathcal{N}(0, 1/\sqrt{N-1}) \quad (\text{B3})$$

for each link ℓ of the network.

This choice of the distribution from which the internal frequencies are drawn implies that the frequencies $\hat{\omega}$ describing the internal frequency of the phases ψ are Gaussian correlated variables with zero mean given by

$$\langle \hat{\omega}_i \rangle = 0, \quad (\text{B4})$$

and covariance matrix of elements given by

$$\mathbf{C}_{ij} = \delta_{ij} - \frac{1}{N-1}. \quad (\text{B5})$$

With these hypotheses the marginal probability $G_1(\hat{\omega})$ that the internal frequency $\hat{\omega}_i$ of a generic node i is given by $\hat{\omega}_i = \hat{\omega}$ can be expressed as (see [25] for the derivation),

$$G_1(\hat{\omega}) = \frac{1}{\sqrt{2\pi/\bar{c}}} \exp\left[-\bar{c}\frac{\hat{\omega}^2}{2}\right], \quad (\text{B6})$$

$$\begin{aligned} & na^{n-1}b^m \partial_t a + ma^n b^{m-1} \partial_t b + i[a^n b^m]n\kappa_\alpha + i[a^n b^m]m\kappa_\beta \\ & + \frac{1}{2}\sigma n [X_\alpha(a^{n+1}b^m) - X_\alpha^*(a^{n-1}b^m)] - \sigma\frac{1}{4}na^n(b^{m+1} - b^{m-1}) \\ & + \sigma\bar{c}\frac{1}{2}m [X_\alpha(a^{n+1}b^m) - X_\alpha^*(a^{n-1}b^m)] + \sigma\frac{1}{2}ma^n(b^{m+1} - b^{m-1}) = 0. \end{aligned} \quad (\text{C1})$$

If the ansatz is correct this equation needs to be satisfied

where we have put

$$\bar{c} = \frac{N}{N-1}. \quad (\text{B7})$$

Appendix C: Derivation of the stationary state expression for a_i and b_i

Let us now consider a given node i and a given continuity Eq. (32). By using the ansatz defined in Eq.(36) and omitting the index i as long as $X_\alpha \neq 0$ we can observe that the continuity Eq. (32) is satisfied if and only if the following equation is satisfied for every $(m, n) \neq (0, 0)$.

for every value of n and m . By putting first $(m, n) = (0, 1)$ and then $(m, n) = (1, 0)$ we get the two equations

$$\begin{aligned} \partial_t a + ia\kappa_\alpha + \frac{1}{2}\sigma [X_\alpha a^2 - X_\alpha^*] - \sigma\frac{1}{4}a(b - b^{-1}) &= 0, \\ \partial_t b + ib\kappa_\beta + \frac{1}{2}\sigma\bar{c} [X_\alpha a - X_\alpha^* a^{-1}] b + \sigma\frac{1}{2}(b^2 - 1) &= 0. \end{aligned} \quad (\text{C2})$$

This shows that if Eqs. (C1) hold then necessarily Eqs. (C2) are satisfied. However it is easy to show that Eqs. (C2) are also a sufficient condition that guarantees that Eqs. (C1) are satisfied for any arbitrary value of n, m . For $X_\alpha = 0$, instead, by proceeding in a similar way we get that a and b satisfy

$$\begin{aligned} \partial_t a + ia\kappa_\alpha - \sigma\frac{1}{4}a(b - b^{-1}) &= 0, \\ \partial_t b + ib\kappa_\beta + \sigma\frac{1}{2}(b^2 - 1) &= 0. \end{aligned} \quad (\text{C3})$$

Appendix D: The onset of the instability of the incoherent phase I

In this Appendix we use stability considerations to derive the synchronization threshold σ_c^* . Let us now consider the first of Eqs. (37) for every $a_i(\omega_i, \hat{\omega}_i)$ and study the stability of the trivial solution in which $a_i(\omega_i, \hat{\omega}_i) = 0$ for every node i , and every choice of the frequencies $(\omega, \hat{\omega})$ implying that also $R_\alpha = 0$. Since $a_i(\omega, \hat{\omega})$ is only a function of $(\omega, \hat{\omega})$ in this section we simplify the notation

omitting the index i . This entails for instance considering the function $a(\omega, \hat{\omega})$ instead of $a_i(\omega_i, \hat{\omega}_i)$, and a similar convention is used for other variables only depending on the node i through the internal frequencies $\omega = \omega_i$ and $\hat{\omega} = \hat{\omega}_i$. To this end we write the first of Eqs. (37) as

$$\partial_t a(\omega, \hat{\omega}) = F(a(\omega, \hat{\omega}), b(\omega, \hat{\omega}), X_\alpha) \quad (\text{D1})$$

with $F(a, b, X_\alpha)$ given by

$$\begin{aligned} F(a, b, X_\alpha) &= -ia\kappa_\alpha - \frac{1}{2}\sigma [X_\alpha a^2 - X_\alpha^*] \\ &+ \sigma\frac{1}{4}a_i(b - b^{-1}), \end{aligned}$$

where $\kappa_\alpha = \kappa_\alpha(\omega, \hat{\omega})$. In this equation X_α is intended to be a function of all the variables \mathbf{a} according to Eqs. (41). By linearizing Eq.(D1) close to the incoherent phase I, i.e. for $a(\omega, \hat{\omega}) = \Delta a(\omega, \hat{\omega}) \ll 1$ for every value of $(\omega, \hat{\omega})$, and neglecting fluctuations in the variables $b(\omega, \hat{\omega})$, we obtain

$$\partial_t \Delta a(\omega, \hat{\omega}) = [-i\kappa_\alpha + \sigma B]\Delta a + \sigma S/2 \quad (\text{D2})$$

where we have defined B as

$$B = \frac{1}{4}(\bar{b} - \bar{b}^{-1}), \quad (\text{D3})$$

with $\bar{b} = \bar{b}(\omega, \hat{\omega})$ indicating the stationary solution of Eq. (37) in the limit $X_\alpha \rightarrow 0$ and $a_j \rightarrow 0$, $\forall i$ and where \mathcal{S} indicates

$$\mathcal{S} = \int d\omega' \int d\hat{\omega}' G_0(\omega') G_1(\hat{\omega}') \Delta a(\omega', \hat{\omega}'). \quad (\text{D4})$$

In order to predict the onset of the instability of the incoherent phase I, i.e. in order to predict the value of σ_c^* we study the discrete spectrum of Eq.(D2). Assuming that Eq. (D2) has Lyapunov exponent λ we get that $\Delta a(\omega, \hat{\omega})$ as

$$\Delta a(\omega, \hat{\omega}) = \frac{1}{2} \mathcal{S} \hat{\Delta}(\omega, \hat{\omega}). \quad (\text{D5})$$

where $\hat{\Delta}(\omega, \hat{\omega})$ is given by

$$\hat{\Delta}(\omega, \hat{\omega}) = \frac{1}{(i\kappa_\alpha + \lambda)/\sigma + B}, \quad (\text{D6})$$

By inserting Eq.(D5) in Eq.(D4) providing the definition of \mathcal{S} , we obtain a self-consistent equation that reads

$$1 = \frac{1}{2} \hat{I} = \frac{1}{2} \int d\omega' \int d\hat{\omega}' G_0(\omega') G_1(\hat{\omega}') \hat{\Delta}(\omega', \hat{\omega}'), \quad (\text{D7})$$

Therefore this equation provides the value of the Lyapunov exponent λ for any given value of the coupling constant σ . We look for the onset of the instability $\sigma = \sigma_c^*$ of the incoherent solution $R_\alpha = 0$ by imposing that its Lyapunov exponent vanishes, i. $\lambda = 0$.

In order to solve this equation we need to find the explicit form for B in the limit $X_\alpha \rightarrow 0$. To this end we consider the second of Eqs. (37) and by considering the stationary solution, we can derive that as $X_\alpha \rightarrow 0$ and $a(\omega, \hat{\omega}) = \Delta a \rightarrow 0$, the variable B is given by

$$B(\omega, \hat{\omega}) = -i \frac{\kappa_\beta}{2\sigma} + \frac{1}{4} \bar{c} \frac{X_\alpha^*}{\Delta a}. \quad (\text{D8})$$

Given that close to the critical point, for $X_\alpha \rightarrow 0$ the order parameter $X_\alpha^* = \mathcal{S}$ and $a(\omega, \hat{\omega})$ is given by Eq.(D5), B can be expressed as

$$B = -i \frac{\kappa_\beta}{2\sigma} + i\bar{c} \frac{1}{4\hat{\Delta}}. \quad (\text{D9})$$

By inserting in this equation the expression of $\hat{\Delta}$ in terms of $\text{Re}B$ and $\text{Im}B$ given by Eq. (D6) we find the explicit form of B in terms of the element of the vector κ

$$B = i \frac{1}{2\sigma} \frac{\bar{c}\kappa_\alpha/2 - \kappa_\beta}{1 + \bar{c}/4}. \quad (\text{D10})$$

We can now insert this expression in $\hat{\Delta}$ finding

$$\hat{\Delta}^{-1} = i \frac{\kappa_\alpha + \kappa_\beta/2}{\sigma(1 + \bar{c}/4)} = i \frac{\omega - \hat{\Omega}}{\sigma} \frac{4 + 2\bar{c}}{4 + \bar{c}}. \quad (\text{D11})$$

In the limit $N \rightarrow \infty$ we have that $\bar{c} \rightarrow 1$ and $\hat{\Omega} \rightarrow \Omega_0$. Therefore in this limit we obtain

$$\hat{\Delta}^{-1} = i \frac{6}{5} \frac{\omega - \Omega_0}{\sigma}. \quad (\text{D12})$$

By using this explicit expression $\hat{\Delta}$ in terms of the frequency of the nodes it is straightforward to see that \hat{I} can be evaluated with the method of residues leading to

$$\hat{I} = \frac{5}{6} \sigma \pi G_0(\Omega_0). \quad (\text{D13})$$

By inserting the values of these integrals in Eq. (D7) we get that the synchronization threshold occurs for

$$\sigma_c^* = \frac{12}{5} \frac{1}{\pi G_0(\Omega_0)}. \quad (\text{D14})$$

In the case in which the frequency of the dynamics associated to the nodes is distributed as a Gaussian distribution $\omega \sim \mathcal{N}(\Omega_0, 1)$ we obtain in the limit $N \rightarrow \infty$ the explicit expression for the synchronization threshold σ_c^* satisfying

$$\sigma_c^* = \frac{12}{5} \sqrt{\frac{2}{\pi}} = 1.91495\dots \quad (\text{D15})$$

Appendix E: The onset of the instability of the coherent phase II

In this Appendix we derive the equations that can be used to numerically determine the value σ_I^* for the onset of the instability of the stationary solution of the continuity equation in phase II. The approach that we describe follows essentially the same steps adopted in the precedent Appendix for the prediction of σ_c^* . However, while in the preceding Appendix the equations are amenable to a fully analytical derivation of σ_c^* , the equations that will be derived in this Appendix can only be solved numerically.

We consider the dynamical equations for $a_i(\omega_i, \hat{\omega}_i)$ and $b_i(\omega_i, \hat{\omega}_i)$ given by Eqs. (37). We notice that the variables $a_i(\omega_i, \hat{\omega}_i)$ and $b_i(\omega_i, \hat{\omega}_i)$ only depend on the index i through the value of its corresponding internal frequencies $\omega = \omega_i$ and $\hat{\omega} = \hat{\omega}_i$. Therefore omitting the index i , the Eqs. (37) can be written as equations for the variable

$$\mathbf{a}(\omega, \hat{\omega}) = \begin{pmatrix} a(\omega, \hat{\omega}) \\ b(\omega, \hat{\omega}) \end{pmatrix} \quad (\text{E1})$$

as

$$\partial_t \mathbf{a}(\omega, \hat{\omega}) = \mathbf{F}(a(\omega, \hat{\omega}), b(\omega, \hat{\omega}), X_\alpha) \quad (\text{E2})$$

where $\mathbf{F}(a, b, X_\alpha)$ is given by

$$\mathbf{F}(a, b, X_\alpha) = \begin{pmatrix} -ia\kappa_\alpha - \frac{1}{2}\sigma [X_\alpha a^2 - X_\alpha^*] + \sigma \frac{1}{4} a(b - b^{-1}) \\ -ib\kappa_\beta - \frac{1}{2}\sigma \bar{c} [X_\alpha a - X_\alpha^* a^{-1}] b - \sigma \frac{1}{2} (b^2 - 1) \end{pmatrix} \quad (\text{E3})$$

and where X_α is given by Eq. (41). Let us develop the dynamical Eq. (E2) close to the stationary solution of phase II when $\mathbf{a} = \bar{\mathbf{a}} + \Delta\mathbf{a}$ with $\bar{\mathbf{a}}$ indicating the stationary solution of Eqs. (E2) in phase II, obtaining

$$\partial_t \mathbf{a} = \mathbf{J}\Delta\mathbf{a} + \mathbf{U}\mathbf{S}. \quad (\text{E4})$$

where \mathbf{J} is the Jacobian matrix

$$\mathbf{J} = \begin{pmatrix} \frac{\partial F_1(a,b,X_\alpha)}{\partial a} & \frac{\partial F_1(a,b,X_\alpha)}{\partial b} \\ \frac{\partial F_2(a,b,X_\alpha)}{\partial a} & \frac{\partial F_2(a,b,X_\alpha)}{\partial b} \end{pmatrix} \quad (\text{E5})$$

calculated at the stationary state corresponding to phase II, and where \mathbf{U} is given by

$$\mathbf{U} = \begin{pmatrix} \frac{\partial F_1}{\partial \text{Re}X_\alpha} & -\frac{\partial F_1}{\partial \text{Im}X_\alpha} & \frac{\sigma}{2} \frac{\partial F_1}{\partial \kappa_\alpha} \\ \frac{\partial F_2}{\partial \text{Re}X_\alpha} & -\frac{\partial F_2}{\partial \text{Im}X_\alpha} & -\sigma \frac{\partial F_2}{\partial \kappa_\beta} \end{pmatrix} \quad (\text{E6})$$

also calculated at the stationary state corresponding to phase II. Moreover by putting

$$\begin{aligned} \Delta a(\omega, \hat{\omega}) &= a_R(\omega, \hat{\omega}) + ia_I(\omega, \hat{\omega}), \\ \Delta b(\omega, \hat{\omega}) &= b_R(\omega, \hat{\omega}) + ib_I(\omega, \hat{\omega}), \end{aligned}$$

we can express the element of the vector $\mathbf{S} = (S_1, S_2, S_3)^\top$ appearing in Eq. (E4) as

$$\begin{aligned} S_1 &= \int d\omega' \int d\hat{\omega}' G_0(\omega') G_1(\hat{\omega}') a_R(\omega', \hat{\omega}'), \\ S_2 &= \int d\omega' \int d\hat{\omega}' G_0(\omega') G_1(\hat{\omega}') a_I(\omega', \hat{\omega}'), \\ S_3 &= \int d\omega' \int d\hat{\omega}' G_0(\omega') G_1(\hat{\omega}') b_I(\omega', \hat{\omega}'). \end{aligned}$$

In order to characterize the value of the coupling constant $\sigma = \sigma_I^*$ for the onset of the instability of the coherent phase II, we study the discrete spectrum of Eq. (E4). Let

us now assume that Eq. (E4) admits λ as its Lyapunov exponent leading to

$$\lambda \Delta\mathbf{a} = \mathbf{J}\Delta\mathbf{a} + \mathbf{U}\mathbf{S}. \quad (\text{E7})$$

Assuming self-consistently that $\mathbf{S} = (S_1, S_2)$ is known, we can express $\Delta\mathbf{a}$ as

$$\Delta\mathbf{a} = \mathbf{H}\mathbf{S} \quad (\text{E8})$$

where \mathbf{H} is a 2×3 matrix given by

$$\mathbf{H} = -[\mathbf{J} - \lambda \mathbf{I}_2]^{-1} \mathbf{U}. \quad (\text{E9})$$

By closing the self-consistent assumption, using the definition of S_1 and S_2 we find the self-consistent system of equations

$$\mathbf{S} = \tilde{\mathbf{I}}\mathbf{S} \quad (\text{E10})$$

with

$$\tilde{\mathbf{I}} = \begin{pmatrix} \text{Re}h_{11} & \text{Re}h_{12} & \text{Re}h_{13} \\ \text{Im}h_{11} & \text{Im}h_{12} & \text{Im}h_{13} \\ \text{Im}h_{21} & \text{Im}h_{22} & \text{Im}h_{23} \end{pmatrix}. \quad (\text{E11})$$

with h_{rs} given by

$$h_{rs} = \int d\omega' \int d\hat{\omega}' G_0(\omega') G_1(\hat{\omega}') H_{rs}(\omega', \hat{\omega}'). \quad (\text{E12})$$

The system of Eqs. (E10) has a non-trivial solution if and only if

$$\det(\tilde{\mathbf{I}} - \mathbf{I}_3) = 0. \quad (\text{E13})$$

In order to evaluate the onset of the instability for phase II we calculate $\det(\tilde{\mathbf{I}} - \mathbf{I}_3)$ as a function of σ when $\lambda = 0$ numerically obtaining a numerical value for σ_I^* which is given by

$$\sigma_I^* = 3.70 \pm 0.05. \quad (\text{E14})$$